

Received: 26 October 2017 Accepted: 20 November 2017 Published online: 22 December 2017

# **OPEN** Anomalous Decay of **Nanomechanical Modes Going Through Nonlinear Resonance**

O. Shoshani<sup>1</sup>, S. W. Shaw<sup>2</sup> & M. I. Dykman<sup>3</sup>

Because of the small size of nanomechanical systems, their vibrations become nonlinear already for small amplitudes. Many nontrivial aspects of the vibration dynamics arise from the coexistence of several nonlinearly coupled modes. We show that such coupling can lead to anomalous decay of the modes where they go through nonlinear resonance, so that their amplitude-dependent frequencies become commensurate. We demonstrate the possibility of a strongly nonmonotonic dependence of the decay rate on the amplitude if one of the modes serves as a thermal reservoir for another mode. Where the decay of both modes is slow compared to the rate of resonant energy exchange, the decay is accompanied by amplitude oscillations. Depending on the initial conditions, with increasing time it can display an extremely sharp or a comparatively smooth crossover between different regimes. The results provide insight into recent experimental results by several groups and suggest new ways of characterizing and controlling nanomechanical systems.

The nonlinear resonance occurs where two vibrational frequencies in the system are commensurate, i.e., their ratio is a rational number. The resonance effects are most pronounced where both the numerator and the denominator of the corresponding fraction are comparatively small integers, for example, where one of the frequencies is twice or three times the other. The study of nonlinear resonance has a long history in quantum and classical mechanics. It goes back at least to Laplace and Poincare on the classical side and to the Fermi resonance on the quantum side<sup>1,2</sup>. The resonance has been observed in a broad range of systems, from celestial bodies to ecological systems to molecules<sup>3-6</sup>. Recently, nonlinear resonance has attracted particular interest in the context of nano- and micro-mechanical vibrational systems<sup>7-15</sup> and microwave cavities used in quantum information <sup>16,17</sup>. These mesoscopic systems provide unprecedented access to studying, using, and controlling this complicated phenomenon.

In conservative classical systems, nonlinear resonance leads to energy oscillations between the resonating modes. This is reminiscent of the energy oscillations between two coupled harmonic oscillators with close frequencies. However, the actual picture in nonlinear resonance is more complicated, extending to dynamical chaos. On the quantum side, nonlinear resonance is in some sense simpler in the absence of dissipation, as its primary signature is the familiar level repulsion.

The quantum situation changes if the resonating modes are dissipative. If the modes have very different decay rates, one of them can serve as a thermal reservoir for another, cf. 18. This effect has been used to drive a slowly decaying microwave cavity mode to a coherent quantum state<sup>16</sup>; it extends to driven modes<sup>19</sup>, and such extension has attracted much attention in cavity optomechanics<sup>20</sup>.

An important advantageous feature of mesoscopic oscillators is the possibility to tune them in and out of nonlinear resonance. This can be done by directly controlling their frequencies<sup>7</sup> or dynamically, using the dependence of the frequency on the vibration amplitude. Here, by driving a mode, one brings its overtone into resonance with an overtone of another mode, which is then also excited. The ensuing backaction significantly changes the dynamics of the driven mode and, in particular, its decay after the driving is switched off. Such decay is a major means of studying mesoscopic vibrational systems<sup>21</sup>.

In this paper we develop a theory of the decay of classical vibrational modes brought into nonlinear resonance. We reveal the rich and unusual pattern of the decay. In particular, if the decay rates of the involved modes are significantly different, the fast decaying mode can be an efficient thermal reservoir for a slowly decaying mode where

<sup>1</sup>Ben-Gurion University of the Negev, Beer-Sheva, 8410501, Israel. <sup>2</sup>Florida Institute of Technology, Melbourne, FL 32901, USA. 3 Michigan State University, East Lansing, MI 48824, USA. Correspondence and requests for materials should be addressed to M.I.D. (email: dykman@pa.msu.edu)

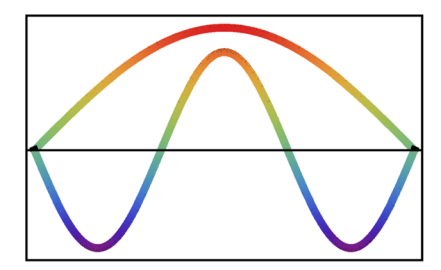


Figure 1. Schematic of 3:1 resonance. Left panel: three excitations (quanta) of mode 1 with frequency  $\omega_1$  can resonantly scatter into an excitation (quantum) of mode 2 with frequency  $\omega_2 \approx 3\omega_1$ , and vice versa, an excitation of mode 2 can resonantly scatter into three excitations of mode 1;  $\gamma_{\rm res}$  is the parameter of the resonant mode coupling. Right panel: a sketch of the first and third flexural modes in a stretched nanowire; these modes are close to 3:1 resonance.

the modes resonate. Since the mode frequencies depend on their amplitudes, the resonance is transient. This leads to a characteristic peak in the instantaneous decay rate of the slowly decaying mode as a function of time. The effect can be thought of as a transient classical analog of the well-known in quantum physics Purcell effect<sup>22</sup>.

The resonant dynamics is very different if the decay rates of both modes are smaller than their nonlinear resonant coupling in the appropriate units. In this case decay is accompanied by comparatively fast energy exchange between the modes that leads to oscillations of the vibration amplitudes. Because the strength of the nonlinear mode coupling strongly depends on the amplitudes, the oscillations are qualitatively different from those in linear resonance. We develop a general framework for analyzing the decay in this situation. It reveals the qualitative features of the decay, including sharp or smooth crossovers between different regimes with varying time. It also allows one to establish the range of parameters and the initial conditions where different types of behavior occur. The approach relies on the existence of a broad parameter range where, as we show, nonlinear dynamics in the absence of decay is much simpler than that in the general Poincare picture of nonlinear resonance in conservative systems <sup>1,23</sup>.

#### Results

**A minimalistic model.** To be specific, we will consider the modes with the frequency ratio close to 3:1, as sketched in Fig. 1. For symmetry reasons, the coupling between such modes in nano- and micromechanical systems is often stronger than the coupling between the modes close to 2:1 resonance. The interesting recent work<sup>14,15</sup>, which has been done in parallel with the present paper, reports the observations of 3:1 resonance and the rich dynamics that come with it.

We describe the modes by the Duffing model, that is conventionally used in nanomechanics<sup>24–26</sup>, complemented by the term that accounts for the resonant nonlinear mode coupling. The Hamiltonian of the system reads

$$H = \sum_{n} \left[ \frac{1}{2} (p_n^2 + \omega_n^2 q_n^2) + \frac{1}{4} \gamma_n q_n^4 \right] + \gamma_{\text{res}} q_1^3 q_2.$$
 (1)

Here,  $q_n$  and  $p_n$  are the coordinate and momentum of mode n (n = 1, 2),  $\omega_{1,2}$  and  $\gamma_{1,2}$  are the mode eigenfrequencies and the Duffing nonlinearity parameters, and  $\gamma_{\rm res}$  is the mode coupling parameter. The model (1) captures the essential features of the resonant behavior.

Nonlinear resonance in nanomechanics is most easily observed where the mode nonlinearity is weak in the sense that the quartic in  $q_n$  terms in H are small compared to the quadratic terms. Therefore 3:1 resonance happens for  $3\omega_1$  close to  $\omega_2$ , so that the frequency difference  $\delta\omega_{12}=3\omega_1-\omega_2$  is small,  $|\delta\omega_{12}|\ll\omega_{1,2}$ . Then the modes can be tuned into exact resonance by varying their vibration amplitudes  $A_{1,2}$  and using that the effective vibration frequency of an nth mode is  $\omega_n^{\rm eff}\approx\omega_n+3\gamma_nA_n^2/8\omega_n^{27}$ . Typically, in the experiment it is the low-frequency mode that is directly excited and tuned into the nonlinear resonance, cf. 7.8,14.15.

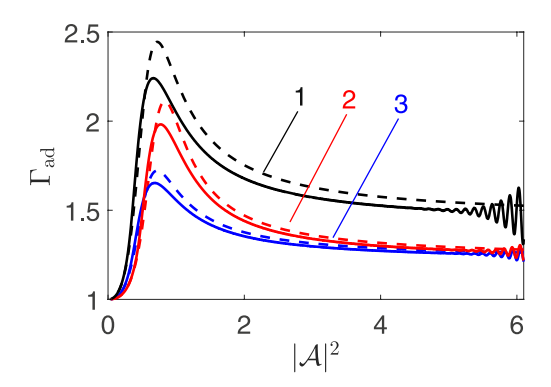
For small  $|\delta\omega_{12}|$ , the amplitude range of interest is where the amplitude-dependent frequency change is small compared to  $\omega_{1,2}$ . This significantly simplifies the analysis, as one can use the rotating wave approximation (RWA) and change from the rapidly oscillating coordinates and momenta of the modes to new scaled coordinates and momenta,  $q_n = \omega_n^{-1/2}(Q_n\cos\phi_n + P_n\sin\phi_n)$ ,  $p_n = -\omega_n^{1/2}(Q_n\sin\phi_n - P_n\cos\phi_n)$  with  $\phi_1 = \omega_1 t$  and  $\phi_2 = 3\omega_1 t$ . Functions  $Q_n$ ,  $P_n$  remain almost constant over time  $1/\omega_1, 1/\omega_2$ . The equations of motion for  $Q_n$ ,  $P_n$  are

$$\dot{Q}_n = -\Gamma_n Q_n + \frac{\partial H_{\text{RWA}}}{\partial P_n}, \quad \dot{P}_n = -\Gamma_n P_n - \frac{\partial H_{\text{RWA}}}{\partial Q_n},$$
 (2)

where  $H_{RWA}$  is the RWA Hamiltonian,

$$H_{\text{RWA}} = -\frac{1}{2}\delta\omega_{12}(Q_2^2 + P_2^2) + \sum_{n} \frac{3\gamma_n}{32\omega_n^2}(Q_n^2 + P_n^2)^2 + \frac{\gamma_{\text{res}}}{8\sqrt{3}\omega_1^2} \text{Re}\left[(Q_1 - iP_1)^3(Q_2 + iP_2)\right]. \tag{3}$$

Whereas the terms with  $H_{\text{RWA}}$  in Eq. (2) come directly from the Hamiltonian (1), the terms  $\propto \Gamma_{1,2}$  have been added to account for mode decay. They come from the linear friction forces  $-2\Gamma_n\dot{q}_n$  experienced by nanomechanical



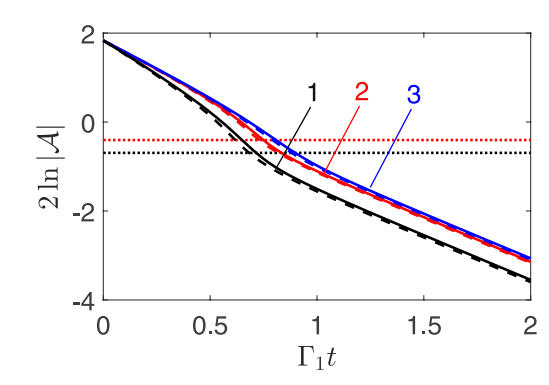


Figure 2. Resonant peak of the instantaneous decay rate. Left panel: The dependence of the normalized effective instantaneous decay rate  $\Gamma_{\rm ad} = -\Gamma_1^{-1}(d/dt) \ln |\mathscr{A}|$  on the scaled vibration amplitude  $|\mathscr{A}|$  of mode 1 in the adiabatic regime of fast decaying mode 2. Right panel: The amplitude of mode 1 in scaled time  $\Gamma_1 t$ ; the horizontal dotted lines indicate the amplitude where the resonance occurs for the respective parameter values,  $3\omega_1^{\rm eff} = \omega_2$  (the black and blue dotted lines overlap). Solid lines are from numerical solution of Eqs (2), and dashed lines are the adiabatic approximation (4). Black, red, and blue curves in both panels (curves 1, 2, and 3) refer to  $\zeta = 4$ ,  $\delta\omega_{12}/\Gamma_2 = -1.5$ ;  $\zeta = 2$ ,  $\delta\omega_{12}/\Gamma_2 = -2$ ; and  $\zeta = 2$ ,  $\delta\omega_{12}/\Gamma_2 = -1.5$ , respectively;  $\Gamma_2/\Gamma_1 = 50$ . The oscillations at large  $|\mathscr{A}|^2$  in the left panel are the effect of the initial conditions where the modes approach the adiabatic regime.

modes. With  $\delta\omega_{12}=3\omega_1-\omega_2$ , the Hamiltonian  $H_{\rm RWA}$  does not contain terms quadratic in  $Q_1,P_1$ . The nonlinear terms disregarded in (3) either renormalize the parameters or lead to corrections that do not change the dynamics qualitatively. Here we aim at revealing most interesting characteristic features of this resonant dynamics.

**Resonant transient nonlinear friction.** Along with the linear friction force, nanomechanical modes often experience nonlinear friction, where the friction coefficient depends on the mode amplitude<sup>28–34</sup>. The microscopic mechanisms considered so far predict that the friction coefficient either monotonically increases<sup>18,35,36</sup>, or decreases<sup>33,37</sup>, with the increasing mode amplitude. In contrast, resonant mode coupling can lead to an anomalously strong nonlinear friction and nonmonotonic amplitude dependence of the friction coefficient.

In systems of coupled nano- and micro-mechanical modes, the higher-frequency modes often decay faster than the lower-frequency ones \$10,38,39\$. In the case of nonlinear resonance, if the higher-frequency mode 2 decays much faster than mode 1,  $\Gamma_2\gg\Gamma_1$ , mode 2 can serve as a thermal reservoir for mode 1. This reservoir is special, as it has a finite bandwidth  $\sim\Gamma_2$ . Therefore it is most efficient only when the amplitude-dependent frequency detuning  $3\omega_1^{\rm eff}-\omega_2^{\rm eff}$  is within this bandwidth. In addition, the coupling to the reservoir is nonlinear in the mode-1 coordinate, which also makes the decay rate of this mode amplitude-dependent.

Other conditions needed for mode 2 to serve as a thermal reservoir for mode 1 and the derivation of the equation of motion for mode 1 are given in Methods. It is convenient to write this equation for a dimensionless complex amplitude of mode 1  $\mathscr{A}=(3\gamma_1/8\omega_1^2\Gamma_2)^{1/2}(Q_1-iP_1)\exp[-i\Phi]$ , where  $\Phi(t)$  is the phase that accumulates due to the amplitude dependence of the mode frequency,  $\dot{\Phi}(t)=\Gamma_2|\mathscr{A}(t)|^2$ ,

$$\dot{\mathcal{A}} = -\Gamma_1 \mathcal{A} \left[ 1 + \frac{\zeta |\mathcal{A}|^4}{1 + i[(\delta \omega_{12}/\Gamma_2) + |\mathcal{A}|^2]} \right]. \tag{4}$$

Here,  $\zeta = (\gamma_{\rm res}/3\gamma_{11})^2\Gamma_2/\Gamma_1$  is the dimensionless characteristic of the strength of the resonant coupling;  $\zeta$  and the ratio  $\delta\omega_{12}/\Gamma_2$  fully determine the decay of the mode amplitude  $A_1 \propto |\mathcal{A}|$  in dimensionless time  $\Gamma_1 t$ .

It is seen from Eq. (4) that the backaction from the fast-decaying mode 2 leads to a nonexponential decay of the amplitude  $A_1$ . The coupling induced decay rate can be understood in terms of the standard Fermi golden rule<sup>40</sup>. It is quadratic in the coupling parameter  $\gamma_{\rm res}$  and is proportional to the "density of states"  $\Gamma_2/[\Gamma_2^2 + (\omega_2 - 3\omega_1^{\rm eff})^2]$  of the effective reservoir provided by mode 2 at triple the frequency of mode 1,  $\omega_1^{\rm eff} = \omega_1 + \Gamma_2|\mathscr{A}|^2$ .

Equation (4) gives in the explicit form the instantaneous decay rate  $(d/dt) \ln |\mathcal{A}|$  as function of the mode-1 amplitude. It is illustrated in Fig. 2. The rate displays a resonant peak for  $3\omega_{\text{leff}} = \omega_2$ , in agreement with the Fermi golden rule. The height of the peak increases with the increasing coupling strength  $\zeta$  and with the increasing frequency detuning  $|\delta\omega_{12}|$ . Interestingly, the rate becomes amplitude-independent not only for small amplitudes, where it approaches the linear-decay value  $\Gamma_1$ , but also for  $|\mathcal{A}|^2 \gg |\delta\omega_{12}|/\Gamma_2$ , where it becomes  $\approx \Gamma_1(1+\zeta/9)$ . The unusual quasi-linear large- $|\mathcal{A}|^2$  behavior is a consequence of the strong increase of the mode coupling with the increasing vibration amplitude. It is clear from (4) and also seen from Fig. 2 that a peak of the decay rate as function of amplitude corresponds to a kink on the time dependence of the amplitude, where the decay rate quickly changes between its values for large and small amplitudes.

**Nonlinear resonance for weak dissipation.** The nontrivial aspects of the dynamics of resonating modes also come forth in the opposite limit, in which the mode relaxation rates are small compared to the rate of the

Figure 3. Phase trajectories of the resonating modes in the absence of decay. Motion along the trajectories (thin black lines) corresponds to oscillations in time of the scaled squared amplitudes I and M-I of modes 1 and 2, respectively, and of the mode phase difference  $\phi$ . The pattern is periodic in  $\phi$  with period  $2\pi$ . The values of the Hamiltonian h, Eq. (5), are color-coded, h is constant on a trajectory. The scaled parameters of the Duffing nonlinearity are  $\mu_1=1$ ,  $\mu_2=0$ , the scaled frequency detuning in (a)–(c) is  $\delta\Omega_{12}/M=-0.5, -0.9, -2$ . The red lines show the separatrices that go into/out of the saddle point. The red crosses in (a) and (b) mark the extrema of h at  $\phi=0$ . The pattern of the trajectories is the same for  $\delta\Omega_{12}\to-\delta\Omega_{12}, \ \mu_1\to-\mu_1, \ \phi\to\phi+\pi$ .

inter-mode energy exchange at resonance. In nano-mechanical systems, all these rates are typically much smaller than the vibration frequencies  $\omega_{1,2}$ . One can then think of the evolution as decay of the vibration amplitudes, accompanied by their oscillations that result from the intermode energy exchange<sup>41</sup>.

The mode dynamics in the absence of decay is interesting on its own and needs to be understood first. The conservative system is characterized by two conserved quantities. The first is the effective energy in the rotating frame and is given by function  $H_{\rm RWA}$  (3). The second is an analog of the Manley-Rowe invariant in nonlinear optics<sup>42</sup> and has the form  $M=I+Q_2^2+P_2^2$  for the considered 3:1 resonance, where  $I=(Q_1^2+P_1^2)/3\equiv\omega_1A_1^2/3$  is the scaled squared amplitude of mode 1. The dynamics is conveniently described by two canonically conjugate variables I and  $\phi$ , where  $\phi=3\arg(Q_1-iP_1)-\arg(Q_2-iP_2)$  is the mode phase difference. In dimensionless time  $\tau=3\gamma_{\rm res}t/4\omega_1^2$  the Hamiltonian equations for these variables read

$$\partial_{\tau}I = -\partial_{\phi}h, \quad \partial_{\tau}\phi = \partial_{I}h; \qquad h(I, \phi) = I\delta\Omega_{12} + \frac{1}{2}\mu_{1}I^{2} + \frac{1}{2}\mu_{2}(M-I)^{2} + I^{3/2}(M-I)^{1/2}\cos\phi.$$
 (5)

Here  $\delta\Omega_{12}=4\omega_1^{~2}\delta\omega_{12}/3\gamma_{\rm res}$ ,  $\mu_1=9\gamma_1/2\gamma_{\rm res}$ , and  $\mu_2=\gamma_2/18\gamma_{\rm res}$  are the dimensionles parameters that determine the dynamics; for brevity, we have set  $\gamma_{\rm res}>0$ .

The effective Hamiltonian  $h \propto H_{\rm RWA}$  is singular for  $I \to M$  and  $I \to 0$ , i.e., in the range where the amplitude of one of the modes goes to zero. This feature is generic for nonlinear resonance in weakly nonlinear oscillators. It leads to the unusual behavior discussed below.

The dynamics (5) can be mapped onto motion of a particle in a potential well and are described by Jacobi elliptic functions; see Supplemental Material (SM). The qualitative insight into the dynamics comes from the phase portraits shown in Fig. 3(a)–(c). They refer to the case where the Duffing nonlinearity of mode 2 can be disregarded,  $\mu_2=0$  (a nonzero  $\mu_2$  does not change the qualitative picture, see SM). The exact nonlinear resonance  $3\omega_1^{\rm eff}=\omega_2^{\rm eff}$  then occurs for  $\delta\Omega_{12}=-\mu_1 I$ . Therefore we concentrate on the case  $\mu_1\delta\Omega_{12}<0$  where the modes can be tuned in resonance by increasing the amplitude of mode 1.

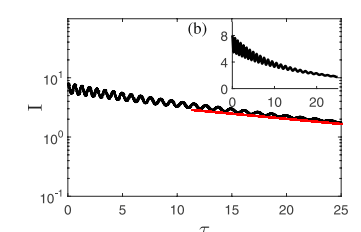
Shown in Fig. 3 are the lines of constant h, which are, essentially, parametric plots of the trajectories  $I(\tau)$ ,  $\phi(\tau)$ . The closed loops correspond to oscillations of I,  $\phi$  about the stationary states where  $h(I,\tau)$  is maximal or minimal. From Eq. (5), the typical dimensional frequency of these oscillations is  $\sim \gamma_{\rm res}/\omega_1^2$ . In contrast, on the open trajectories  $\phi(\bmod{2\pi})$  runs from  $-\pi$  to  $\pi$ . These trajectories correspond to accumulation of phase  $\phi$  in time, which is also accompanied by oscillations of the mode amplitudes. We note that, in the absence of resonant mode coupling, the phase trajectories are just straight horizontal lines, as in this case the amplitudes of the modes are constant on times small compared to the decay time.

The closed trajectories circling around different extrema of h are separated from each other and from the open trajectories by separatrices. A peculiar feature of the system is that, in contrast to the "conventional" picture of a phase plane<sup>1</sup>, there are two types of separatrices (Methods). Of particular importance are the separatrices shown by red lines in Fig. 3(a) and (b), which go to/from the saddle point of  $h(I, \phi)$  (SM). This point is a stationary state,  $\partial_{\tau}I = \partial_{\tau}\phi = 0$ . However, rather than circling it, the nearby trajectories approach and then move away, except for the separatrices.

It is important to note the change of the phase portrait from panel (a) to (c) in Fig. 3. With the increasing ratio  $|\delta\Omega_{12}|/M$ , the saddle point and the extremum of h (at  $\phi=0$  for  $\mu_1>0$ ) move closer to each other. Ultimately they merge (the saddle-node bifurcation<sup>1</sup>) and disappear. As the extremum disappears, the trajectories that circled it transform into open trajectories.

In the presence of decay, h and M are no longer conserved. However, they vary in time slowly compared to the oscillation period. One can therefore think of the dynamics as described by Eq. (5) with slowly evolving h and M. From Eq. (2), time evolution of the Manley-Rowe parameter  $M = \omega_1 A_1^2 / 3 + \omega_2 A_2^2$  is described by the equation

$$\langle \dot{M} \rangle = -2\Gamma_2 M + 2(\Gamma_2 - \Gamma_1) \langle I \rangle,$$
 (6)



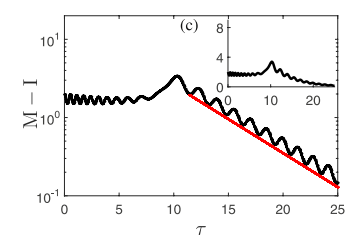


Figure 4. Time evolution of the amplitudes of the modes for small decay rates. The scaled squared amplitudes  $I=\omega_1A_1^2/3$  [panels (a) and (b)] and  $M-I=\omega_2A_2^2$  [panel (c)] of modes 1 and 2, respectively, are shown as functions of the scaled time  $\tau=3\gamma_{\rm res}t/4\omega_1^2$ . The main figures are on the logarithmic scale, the red lines show the exponential decay of I and M-I in the small-amplitude limit. The insets show the time evolution on the linear scale. The parameters are  $\delta\Omega_{12}=-5$ ,  $\mu_1=1$ , and M(0)=10, which corresponds to the parameter values in Fig. 3(a). The initial values of the phase  $\phi(0)=0$  in panels (a) and (c),  $\phi(0)=\pi$  in panel (b), and I(0)=8 correspond to the trajectories that start near the centers at  $\phi=0$  and  $\phi=\pi$  in Fig. 3(a). The decay rates are  $4\omega_1^2\Gamma_1/3\gamma_{\rm res}=0.02$ ,  $\Gamma_2/\Gamma_1=5$ .

where the angular brackets denote time averaging over the period of motion with given h and M. A similar equation can be written for  $\langle h \rangle$  (Methods).

From Eq. (6) and the condition  $M-I \ge 0$ , M monotonically decreases in time. Physically, this is a consequence of the decrease of the energy of the coupled modes. As M decreases, the ratio  $|\delta\Omega_{12}|/M$  increases. Therefore Fig. 3(a) to (c) can be thought of as the snapshots of the phase portrait at successive times (disregarding the nonqualitative modification of the phase portrait due to the decay). They refer to the most interesting case where, initially,  $|\delta\Omega_{12}|/M$  is small and the system has two well separated centers and a saddle point [Fig. 3(a)]; with increasing time, one of the centers and the saddle point move closer to each other [Fig. 3(b)]; still later, these points merge and disappear [Fig. 3(c)].

From the above arguments, the time evolution of the squared vibration amplitude  $A_1^2 \propto I$  can follow qualitatively distinct routes depending on the initial conditions. Samples of this evolution are shown in Fig. 4 for two extreme cases, where the initial values of the mode amplitudes and phases are close to different extrema of h, i.e., to different centers in Fig. 3 (see SM for an intermediate case). In the presence of dissipation, the closed orbits in Fig. 3 become spirals. As the system moves along a spiral trajectory,  $I(\tau)$  oscillates, whereas  $\langle I(\tau) \rangle$  slowly decays. This behavior is common to the initial portion of the traces in Fig. 4(a),(b).

The functions  $I(\tau)$  become qualitatively different as the increasing  $|\delta\Omega_{12}|/M$  approaches the value where one of the extrema of h disappears (in the considered case, that at  $\phi=0$  in Fig. 3). Here, the orbit that initially circulated about this extremum dramatically changes, see Fig. 4(a). The value of I sharply drops. We find that, after the transient, the system evolves along an open orbit in Fig. 3, that is slightly modified by the dissipation and has a comparatively small I/M. The scaled squared amplitude I oscillates and  $\langle I \rangle$  decays, but with a different decrement than above the bifurcation point. In contrast, the orbit that started near the other extremum of h (at  $\phi=\pi$ ), keeps oscillating, with  $\langle I \rangle$  decaying smoothly, although the decay is nonexponential, except for small I, see Fig. 4(b).

The sharp change of I is a consequence of the change of the topology of the phase portrait. It occurs near resonance where  $3\omega_1^{\rm eff}=\omega_2^{\rm eff}$  and is not related to the ratio of the mode decay rates (SM). Naturally, it is not described by the method of averaging<sup>43</sup> (we remind that the averaging here is done in the rotating frame). As seen from Fig. 4(c), the drop of the squared amplitude of mode 1 can be accompanied by the increase of the squared amplitude  $A_2^2=\omega_2^{-1}(M-I)$  of mode 2 (Methods).

The nontrivial time evolution of the amplitude of the low-frequency mode in 3:1 resonance was carefully studied in the experiments <sup>14,15</sup>, and through simulations <sup>14</sup>. It was discovered that the mode decay is accompanied by amplitude oscillations. However, their employed methods did not allow revealing the sharp drop of  $I(\tau)$  between different regimes of decaying oscillations and the mechanism of this effect, as well as the qualitative difference of the behavior of I(t) depending on the initial conditions.

#### Discussion

The results of this paper show the rich dynamics of micro- and nanomechanical systems in which vibrational modes experience nonlinear resonance. The features of the dynamics come from the separation of the time scales of the fast vibrations and the comparatively slow evolution of their amplitudes and phases, which are themselves controlled by the interplay of the modes' nonlinearity, decay, and the nonlinear resonant coupling. These features make the dynamics different from the conventional dynamics of nonlinear resonance and the already complicated dynamics of individual nonlinear modes in the absence of resonance.

Unexpected behavior can be seen by following the mode decay in time, which is a basic tool in the studies of micro- and nano-mechanical systems. Our specific results refer to the decay of the modes that are close to 3:1 resonance, but the revealed behavior is common for internal resonance of weakly damped modes (Methods).

Because of the nonlinear resonance, the decay of vibrational modes becomes strongly non-exponential, with a decay rate that depends on the vibration amplitude, sometimes in a non-monotonic manner. This is a consequence of the amplitude dependencies of the coupling strength and the mode frequencies, which lead to tuning the modes into and out of resonance as their amplitudes vary. The effect is described explicitly in an important case where the high-frequency mode decays much faster than the low-frequency one. Here, the high-frequency

mode serves as a thermal reservoir for the low-frequency mode. The results can be understood in terms of an effective transient Purcell effect, or an anomalous nonlinear friction, with a pronounced peak in the dependence of the friction coefficient on the mode amplitude.

A very unusual behavior occurs if the decay rates of the modes are small compared to the appropriately scaled nonlinear coupling. Here, the decay of the vibration amplitude is accompanied by oscillations with a frequency determined by the nonlinear coupling. This frequency is much smaller than the mode frequencies  $\omega_{1,2}$ , but can be much higher than the decay rate. Depending on the initial conditions, the oscillations can be qualitatively different. They may smoothly decay along with the mean value of the amplitude. However, unexpectedly, the amplitude can also experience a steep crossover between regimes in which both the magnitude of the oscillations and the mean value of the amplitude are significantly different. Such a jump is a consequence of the change of the topology of the phase portrait in the absence of decay, which is generic for resonating nanomechanical modes.

The features of the nonlinear resonance found in this paper, including the transient Purcell effect and the sharp switching between different regimes of decay, provide insight into existing experimental observations in nano- and micro-mechanical systems and suggest new experiments. The results also suggest new ways of extracting the parameters of the systems and of controlling transient processes in nanomechanics.

#### Methods

The calculations in the paper are done for the Duffing nonlinearity parameter  $\gamma_1>0$ . In this case the modes are tuned in resonance with increasing amplitude  $A_1$  for  $\delta\omega_{12}<0$ . A generalization to  $\gamma_1<0$ ,  $\delta\omega_{12}>0$  is straightforward.

**Resonant nonlinear friction.** For  $\Gamma_2 \gg \Gamma_1$ , mode 2 follows mode 1 adiabatically. In the adiabatic approximation, one solves the equation of motion for mode 2 by introducing its complex scaled amplitude  $\mathcal{B} = (Q_2 - iP_2) \exp[-3i\Phi(t)]$  and disregarding in Eq. (2)  $d\mathcal{B}/dt$  compared to  $\Gamma_2\mathcal{B}$ . This results in a linear algebraic equation for  $\mathcal{B}$ . Its solution gives Eq. (4). Such analysis disregards the frequency shift of mode 2 due to its Duffing nonlinearity, which is justified for large  $\Gamma_2$ . This explains why Eq. (4) contains  $\omega_2$  rather than  $\omega_2^{\text{eff}}$ . Equation (4) applies if  $|\dot{A}| \ll \Gamma_2 |\mathcal{A}|$ . This imposes a constraint on the strength of the resonant mode coupling for which the adiabatic approximation holds,  $\zeta \delta \omega_{12}^2/\Gamma_2^2 \ll \Gamma_2/\Gamma_1$ .

which the adiabatic approximation holds,  $\zeta \, \delta \omega_{12}^2 / \Gamma_2^2 \ll \Gamma_2 / \Gamma_1$ . The nonexponential decay described by Eq. (4) can be explcitily illustrated for comparatively small amplitudes or strong detuning  $|\delta \omega_{12}|$ , where in (4)  $\omega_1^{\rm eff}$  can be replaced with  $\omega_1$ . Then for the scaled squared vibration amplitude  $e(t) = \left[\zeta/(1+(\delta \omega_{12}/\Gamma_2)^2)\right]^{1/2} |\mathcal{A}(t)|^2$  one obtains

$$e(t) = e(0) \exp(-2\Gamma_1 t) \{1 + e^2(0)[1 - \exp(-4\Gamma_1 t)]\}^{-1/2}$$

The decay of e(t) is faster than exponential, and becomes exponential only for large time, where  $e(t) \ll 1$ . We note the difference of the functional form of e(t) from the decay for nonresonant nonlinear friction <sup>18,24</sup>.

Along with dissipation, the backaction from the mode coupling leads to a change of the effective vibration frequency,  $\omega_1^{\rm eff} \to \omega_1^{\rm eff} + \Delta\omega_1$ , which in turn leads to a change of the phase of  $\mathscr A$ . From Eq. (4),  $\Delta\omega_1 = -\Gamma_1\zeta|\mathscr A|^4 {\rm Im}\{[1+i(3|\mathscr A|^2+\delta\omega_{12}/\Gamma_2)]^{-1}\}$ . The shift  $\Delta\omega_1$  is a nonlinear counterpart of frequency anti-crossing for strong damping  $\Gamma_2$ . It is a strongly nonlinear function of the vibration amplitude, which changes sign for  $3\omega_1^{\rm eff}=\omega_2$ . The latter may lead to a kink on the dependence of the overall mode-1 frequency  $\omega_1^{\rm eff}+\Delta\omega_1$  on the scaled amplitude  $|\mathscr A|$ .

A resonant peak of the decay rate as function of the mode amplitude emerges also for 2:1 resonance. If  $\omega_2$  is close to  $2\omega_1$ , the dynamics of resonantly coupled modes in the rotating frame are described by Eqs (2) and (3) with the coupling term  $\propto \gamma_{\rm res}$  in  $H_{\rm RWA}$  replaced with  $(\beta_{\rm res}/2\omega_1){\rm Re}\,[(Q_1-iP_1)^2(Q_2+iP_2)]$ . For  $\Gamma_2\gg\Gamma_1$  the resonant nonlinear friction is described by equation

$$\dot{\mathcal{A}} = -\Gamma_{1}\mathcal{A}\left[1 + \frac{{\zeta'}_{\mathrm{res}}|\mathcal{A}|^{2}}{1 + i(2\omega_{1}^{\mathrm{eff}} - \omega_{2})/\Gamma_{2}}\right]$$

with  $\zeta'_{\text{res}} = 4\beta_{\text{res}}^2/3\gamma_1$ . As seen from this equation, the decay for 2:1 resonance is similar to that for 3:1 resonance. We note, however, that in this case the decay rate approaches its linear value at both small and large amplitudes.

**The decay-free dynamics.** The conservative dynamics of the coupled modes in the RWA differs from the conventional picture of nonlinear resonance in the action-angle variables  $^{23}$ . In Eq. (5), the effective "action" variable I is limited,  $0 \le I \le M$ . For  $I \to M$  the dynamics becomes singular,  $|\partial_{\tau}\phi| \to \infty$ . The points  $(\phi = (2n+1)\pi/2, I \to M)$  separate regions where  $\partial_{\tau}\phi$  has opposite signs, and the nearby trajectories move in opposite directions along the  $\phi$ -axis. In particular, they can spin around different centers, as in Fig. 3. There is no slowing down near these points. On a trajectory that at  $\tau = 0$  goes through a point  $\phi_0 = \pi/2 - \varepsilon_{\phi}$ ,  $I_0 = M(1 - \varepsilon_I)$  with small  $|\varepsilon_{\phi}|$  and  $\varepsilon_I$ , we have  $\tan \phi(\tau) \approx \varepsilon_{\phi}^{-1} - M\tau/(2\varepsilon_I^{1/2}\varepsilon_{\phi})$  for  $\tau \lesssim \varepsilon_I^{1/2}/M$ . The time  $\varepsilon_I^{1/2}/M$  is the typical dimensionless time to go over the phase interval  $\pi$  for small M-I.

In the presence of weak dissipation, the effective Hamiltonian h is no longer conserved and ultimately decays to zero, along with the Manley-Rowe invariant M. From Eq. (2), for  $\mu_2 = 0$  the period-averaged rate at which h changes is

$$\langle \dot{h} \rangle = -2\Gamma_1 \langle I \dot{\phi} \rangle + \frac{1}{2} \left\langle \frac{I^{3/2} \dot{M}}{(M-I)^{1/2}} \cos \phi \right\rangle \tag{7}$$

(note that the derivatives here and in Eq. (6) are taken with respect to dimensional time t). Equations (6) and (7) apply for h sufficiently far from from its saddle-point value, so that the period of motion with constant h and M is small compared to the reciprocal decay rates  $\Gamma_{1,2}^{-1}$ . In contrast to the Manley-Rowe invariant M, the evolution of h may be nonmonotonic.

The anomalous behavior of the squared amplitude of mode 2,  $A_2^2 = \omega_2^{-1}(M-I)$ , in the presence of dissipation shown in Fig. 4(c), can be understood from Eq. (6). If  $\Gamma_2 \gg \Gamma_1$  and  $\langle I \rangle$  varies on a time scale longer than  $1/\Gamma_2$ , as in the initial section of Fig. 4(a), the quasistationary solution of Eq. (6) is  $M - \langle I \rangle \approx -(2\Gamma_1\langle I \rangle + \langle I \rangle)/2\Gamma_2$ . Therefore  $\langle A_2^2 \rangle$  remains small and weakly varies before the drop of I. The drop of I is associated with a fast switching between different quasiperiodic orbits. Therefore M-I can increase where I drops. Physically, this increase corresponds to a resonant energy transfer from mode 1 to mode 2. This process is not described by the averaging method and by the quasistationary solution, there is no time scale separation between oscillations with given I and the decay.

#### References

- 1. Arnold, V. I. Mathematical Methods of Classical Mechanics (Springer, New York, 1989).
- 2. Fermi, E. The Raman effect of carbon dioxide. Zeitschrift Fur Physik 71, 250-259, https://doi.org/10.1007/BF01341712 (1931).
- 3. Nayfeh, A. H., Mook, D. T. & Marshall, L. R. Nonlinear coupling of pitch and roll modes in ship motions. *Journal of Hydronautics* 7, 145–152 (1973).
- 4. Alfriend, K. Stability and motion in two degree-of-freedom hamiltonian systems for two-to-one commensurability. *Celestial mechanics* 3, 247–265 (1971).
- 5. Blasius, B., Huppert, A. & Stone, L. Complex dynamics and phase synchronization in spatially extended ecological systems. *Nature* **399**, 354–359 (1999).
- 6. Nakamoto, K. Infrared and Raman Spectra of Inorganic and Coordination Compounds: Part A: Theory and Applications in Inorganic Chemistry (Wiley, 2008).
- 7. Eichler, A., del Ålamo Ruiz, M., Plaza, J. A. & Bachtold, A. Strong coupling between mechanical modes in a nanotube resonator. *Phys. Rev. Lett.* **109**, 025503 (2012).
- 8. Antonio, D., Zanette, D. H. & Lopez, D. Frequency stabilization in nonlinear micromechanical oscillators. *Nature Communications* 3, 806 (2012).
- 9. Matheny, M. H., Villanueva, L. G., Karabalin, R. B., Sader, J. E. & Roukes, M. L. Nonlinear mode-coupling in nanomechanical systems. *Nano Lett.* 13, 1622–1626 (2013).
- Mahboob, I., Nishiguchi, K., Fujiwara, A. & Yamaguchi, H. Phonon lasing in an electromechanical resonator. Phys. Rev. Lett. 110, 127202, https://doi.org/10.1103/PhysRevLett.110.127202 (2013).
- 11. Qalandar, K. et al. Frequency division using a micromechanical resonance cascade. Applied Physics Letters 105, 244103 (2014).
- Nitzan, S. H. et al. Self-induced parametric amplification arising from nonlinear elastic coupling in a micromechanical resonating disk gyroscope. Scientific reports 5 (2015).
- 13. Mangussi, F. & Zanette, D. H. Internal resonance in a vibrating beam: A zoo of nonlinear resonance peaks. PLOS One 11, e0162365 (2016).
- 14. Güttinger, J. et al. Energy-dependent path of dissipation in nanomechanical resonators. Nat. Nano. 12, 631 (2017).
- 15. Chen, C., Zanette, D. H., Czaplewski, D. A., Shaw, S. & López, D. Direct observation of coherent energy transfer in nonlinear micromechanical oscillators. *Nat. Comm.* **8**, 15523 (2017).
- 16. Leghtas, Z. et al. Confining the state of light to a quantum manifold by engineered two-photon loss. Science 347, 853-857 (2015).
- 17. Wang, C. et al. A Schrödinger cat living in two boxes. Science 352, 1087-1091, https://doi.org/10.1126/science.aaf2941 (2016).
- 18. Dykman, M. I. & Krivoglaz, M. A. Spectral distribution of nonlinear oscillators with nonlinear friction due to a medium. *Phys. Stat. Sol. (b)* 68, 111–123 (1975).
- Dykman, M. I. Heating and cooling of local and quasilocal vibrations by non-resonance field. Sov. Phys. Solid State 20, 1306–1311 (1978).
- 20. Aspelmeyer, M., Kippenberg, T. J. & Marquardt, F. Cavity optomechanics. Rev. Mod. Phys. 86, 1391 (2014).
- 21. Sansa, M. et al. Frequency fluctuations in silicon nanoresonators. Nat. Nanotech. 11, 552 (2016).
- 22. Purcell, E. M. Spontaneous emission probabilities at radio frequencies. *Phys. Rev.* **69**, 681, https://doi.org/10.1103/PhysRev.69.674 (1946)
- 23. Lichtenberg, A. J. & Lieberman, M. A. Regular and Chaotic Dynamics (Springer, New York, 1992).
- Lifshitz, R. & Cross, M. C. Nonlinear dynamics of nanomechanical and micromechanical resonators. In Schuster, H. G. (ed.) Review of Nonlinear Dynamics and Complexity, 1–52 (Wiley, Weinheim, 2008).
- 25. Eom, K., Park, H. S., Yoon, D. S. & Kwon, T. Nanomechanical resonators and their applications in biological/chemical detection: Nanomechanics principles. *Phys. Rep.* **503**, 115–163 (2011).
- Dykman, M. I. (ed.) Fluctuating Nonlinear Oscillators: from Nanomechanics to Quantum Superconducting Circuits (OUP, Oxford, 2012).
- 27. Landau, L. D. & Lifshitz, E. M. Mechanics. 3rd edn (Elsevier, Amsterdam, 2004).
- 28. Eichler, A. et al. Nonlinear damping in mechanical resonators made from carbon nanotubes and graphene. Nature Nanotech. 6, 339–342 (2011).
- 29. Zaitsev, S., Shtempluck, O., Buks, E. & Gottlieb, O. Nonlinear damping in a micromechanical oscillator. *Nonlinear Dynamics* **67**, 859 (2012).
- 30. Imboden, M., Williams, O. A. & Mohanty, P. Observation of nonlinear dissipation in piezoresistive diamond nanomechanical resonators by heterodyne down-mixing. *Nano Lett.* 13, 4014–4019, https://doi.org/10.1021/nl401978p (2013).
- 31. Miao, T. F., Yeom, S., Wang, P., Standley, B. & Bockrath, M. Graphene nanoelectromechanical systems as stochastic-frequency oscillators. *Nano Lett.* 14, 2982–2987, https://doi.org/10.1021/nl403936a (2014).
- 32. Mahboob, I. *et al.* Dispersive and dissipative coupling in a micromechanical resonator embedded with a nanomechanical resonator. *Nano Lett.* **15**, 2312–2317 (2015).
- 33. Singh, V., Shevchuk, O., Blanter, Y. M. & Steele, G. A. Negative nonlinear damping of a multilayer graphene mechanical resonator. *Phys. Rev. B* **93**, 245407, https://doi.org/10.1103/PhysRevB.93.245407 (2016).
- 34. Polunin, P. M., Yang, Y., Dykman, M. I., Kenny, T. W. & Shaw, S. W. Characterization of mems resonator nonlinearities using the ringdown response. *Journal of Microelectromechanical Systems* 25, 297–303 (2016).

- Croy, A., Midtvedt, D., Isacsson, A. & Kinaret, J. M. Nonlinear damping in graphene resonators. *Phys. Rev. B* 86, 235435, https://doi. org/10.1103/PhysRevB.86.235435 (2012).
- 36. Atalaya, J., Kenny, T. W., Roukes, M. L. & Dykman, M. I. Nonlinear damping and dephasing in nanomechanical systems. *Phys. Rev. B* **94**, 195440 (2016).
- 37. Gao, J. et al. A semiempirical model for two-level system noise in superconducting microresonators. Appl. Phys. Lett. 92, 212504 (2008)
- 38. Patil, Y. S., Chakram, S., Chang, L. & Vengalattore, M. Thermomechanical two-mode squeezing in an ultrahigh-Q membrane resonator. *Phys. Rev. Lett.* 115, 017202, https://doi.org/10.1103/PhysRevLett.115.017202 (2015).
- 39. Sun, F., Dong, X., Zou, J., Dykman, M. I. & Chan, H. B. Correlated anomalous phase diffusion of coupled phononic modes in a sideband-driven resonator. *Nature Commun.* 7, 12694 (2016).
- 40. Landau, L. D. & Lifshitz, E. M. Quantum mechanics. Non-relativistic theory, 3rd edn (Butterworth-Heinemann, Oxford, 1997).
- 41. Vakakis, A. F. et al. Nonlinear targeted energy transfer in mechanical and structural systems, vol. 156 (Springer, Berlin, 2008).
- 42. Boyd, R. W. Nonlinear Optics, 3rd edn (Elsevier, Amsterdam, 2008).
- 43. Neishtadt, A. I. Averaging passage through resonances, and capture into resonance in two-frequency systems. *Russian Mathematical Surveys* **69**, 771–843, https://doi.org/10.1070/RM2014v069n05ABEH004917 (2014).

#### Acknowledgements

We are grateful to Adrian Bachtold, Andreas Isacsson, Daniel López, Pavel Polunin, and Scott Strachan for fruitful discussions. This work was supported in part by the US Defense Advanced Research Projects Agency (FA8650-13-1-7301). SWS acknowledges partial support from the National Science Foundation (Grants No.CMMI 1561934 and CMMI 1662619). OS and SWS were supported in part by Florida Institute of Technology. MID acknowledges partial support from the National Science Foundation (Grants No. DMR-1514591 and CMMI-1661618).

#### **Author Contributions**

MID and SWS formulated the problem. All authors participated in the analysis, with MID and OS developing primarily the analytical approaches and OS and SWS concentrating primarily on numerical simulations. All authors co-wrote the paper."

#### **Additional Information**

Supplementary information accompanies this paper at https://doi.org/10.1038/s41598-017-17184-6.

**Competing Interests:** The authors declare that they have no competing interests.

**Publisher's note:** Springer Nature remains neutral with regard to jurisdictional claims in published maps and institutional affiliations.

Open Access This article is licensed under a Creative Commons Attribution 4.0 International License, which permits use, sharing, adaptation, distribution and reproduction in any medium or format, as long as you give appropriate credit to the original author(s) and the source, provide a link to the Creative Commons license, and indicate if changes were made. The images or other third party material in this article are included in the article's Creative Commons license, unless indicated otherwise in a credit line to the material. If material is not included in the article's Creative Commons license and your intended use is not permitted by statutory regulation or exceeds the permitted use, you will need to obtain permission directly from the copyright holder. To view a copy of this license, visit <a href="https://creativecommons.org/licenses/by/4.0/">https://creativecommons.org/licenses/by/4.0/</a>.

© The Author(s) 2017

# SUPPLEMENTAL MATERIAL:

# Anomalous Decay of Nanomechanical Modes Going Through Nonlinear Resonance

O. Shoshani, S. W. Shaw, and M. I. Dykman

The effective Hamiltonian in the absence of dissipation. Fig. 1 shows the effective Hamiltonian of the resonating nonlinearly coupled modes  $h(I, \phi)$  as function of the scaled squared amplitude of mode 1,  $I = \omega_1 A_1^2/3$ , and the phase difference between the modes  $\phi$ . The Hamiltonian is given by Eq. (5) of the main text, which we reproduce here for completeness,

$$h(I,\phi) = I\delta\Omega_{12} + \frac{1}{2}\mu_1 I^2 + \frac{1}{2}\mu_2 (M-I)^2 + I^{3/2} (M-I)^{1/2} \cos\phi$$
 (1)

It is clear from Eq. (1) that the internal nonlinearity of mode 2, which is characterized by the parameter  $\mu_2$  can be incorporated into the analysis by renormalizing

$$\mu_1 \to \mu_1 + \mu_2, \ \delta\Omega_{12} \to \delta\Omega_{12} - \mu_2 M, \ h \to h + \frac{1}{2}\mu_2 M^2$$
 (2)

Equation (2) shows that much of the qualitative features of the dynamics can be captured by setting  $\mu_2 = 0$ , as it is done in the main text and in the analysis below.

For the chosen signs of the parameters in Fig. 1,  $\delta\Omega_{12} < 0$  and  $\mu_1 > 0$ , function  $h(I,\phi)$  has a minimum for  $\phi(\text{mod }2\pi) = \pi$  and a maximum for  $\phi(\text{mod }2\pi) = 0$ . Also clearly seen is a saddle point  $h_S$  for  $\phi_S(\text{mod }2\pi) = 0$  and  $(I/M)_S \approx 0.18$ : the curvature at the saddle point is positive along the I-axis and negative along the  $\phi$ -axis.

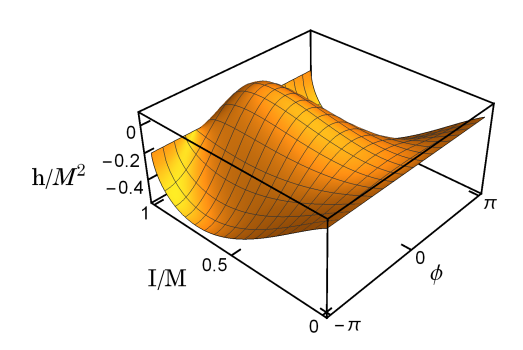


**Figure 1.** The scaled Hamiltonian  $h(I,\phi)/M^2$  of the coupled modes in the absence of decay. The scaling factor M is related to the mode amplitudes  $A_{1,2}$  as  $M=\omega_2A_2^2+I$ , with  $I=\omega_1A_1^2/3$ . The plot refers to the following parameter values in Eq. (1):  $\delta\Omega_{12}/M=-0.7$ ,  $\mu_1=1$ ,  $\mu_2=0$ .

The trajectories in Fig. 3 of the main text are the cross-sections of the surface  $h(I,\phi)$  by the planes h= const. Figure 1 shows that the cross-sections with the values of h near the minimum of  $h(I,\phi)$  are closed contours (the closed loops in the blue area in Fig. 3 of the main text). A cross-section for the saddle-point value of the Hamiltonian  $h=h_S$  gives a closed loop around the maximum and also an open contour where  $\phi$  varies across the whole range of periodicity  $(-\pi,\pi)$ , cf. the red trajectory in Figs. 3(a),(b) of the main text. The cross-section for the values of h between  $h_S$  and the maximum of  $h(I,\phi)$  represent closed contours centered around the maximum, and open contours, as seen in Fig. 3 of the main text.

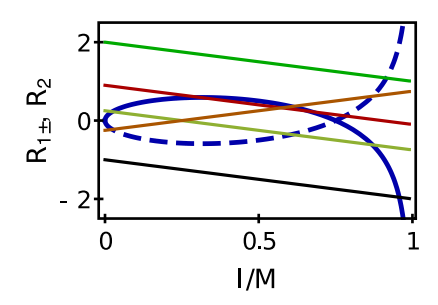


Figure 2. Change of the topology of the phase portrait with the varying Manley-Rowe parameter. The functions  $R_{1\pm}(I/M)$ , Eq. (3), are shown by dark blue lines (the signs "+" and "-" refer to the solid and dashed line, respectively). The straight lines with negative slope give  $R_2(I/M)$  for  $\mu_1 = 1$ . The parameter  $\delta\Omega_{12}/M$  from top to bottom is -2, -0.9, -0.25, 1 (the green, red, light green, and black lines, respectively). The straight brown line with positive slope gives  $R_2$  for  $\mu_1 = -1$  and  $\delta\Omega_{12}/M = -0.25$ . The intersections of the straight lines with the solid and dashed blue lines give the values of I/M at the stationary states for  $\phi = 0$  and  $\phi = \pi$ , respectively. The number of intersections, and thus the topology of the phase portrait, change with varying  $\delta\Omega_{12}/M$ 

The change of the topology of the phase portrait due to decay. An important insight into the dynamics in the presence of decay comes from Fig. 2, which complements the previous analysis. This figur allows findin the location of the stationary states of the Hamiltonian dynamics  $\partial_I h = \partial_{\phi} h = 0$  and following their evolution in time due to decay. Such evolution includes the coalescence of the saddle point and an extremum of  $h(I, \phi)$  (the saddle-node bifurcation), which leads to the dramatic change of the mode amplitudes discussed in the main text.

From Eq. (1), the stationary states (the extrema and the saddle point) of  $h(I,\phi)$  are located at  $\phi(\text{mod}\,2\pi)=0$  and  $\phi(\text{mod}\,2\pi)=\pi$ . Their positions along the *I*-axis are given by equation  $\partial_I h=0$  evaluated for  $\phi=0$  and  $\phi=\pi$ . This equation can be conveniently written as  $R_{1\pm}(I/M)=R_2(I/M)$ , where

$$R_{1\pm}(x) = \pm \frac{(3-4x)\sqrt{x}}{2\sqrt{1-x}}, \quad R_2(x) = -\frac{\delta\Omega_{12}}{M} - \mu_1 x$$
 (3)

Functions  $R_{1\pm}(I/M)$ ,  $R_2(I/M)$  are shown in Fig. 2. Function  $R_{1\pm}$  has no parameters. In contrast, the slope of  $R_2(I/M)$  depends on  $\mu_1$ , whereas  $R_2(0)$  is given by  $-\delta\Omega_{12}/M$ . It is seen from the figur that the number of intersections of  $R_{1\pm}$  and  $R_2$ , i.e., the number of the stationary states of the Hamiltonian system, sensitively depends on  $\delta\Omega_{12}/M$  and  $\mu_1$ . The system has three stationary states for not too large  $|\delta\Omega_{12}|/M$ , but as this parameter increases beyond a critical value (which depends on  $\mu_1$ ), there remains only one stationary state. The critical value of  $|\delta\Omega_{12}|/M$  determines the point where the corresponding extremum of  $h(I,\phi)$  merges with the saddle and disappears. Respectively, the topology of the phase portrait of the Hamiltonian system described by Eq. (1) changes from that in Figs. 3(a) and (b) of the main text to that in Fig. 3(c).

As explained in the main text, the change of the number of the stationary states at the saddle-node bifurcation can lead to a dramatic change of the time dependence of the scaled vibration amplitude I. The fact that, due to decay, the Manley-Rowe invariant M monotonically decreases shows that the ratio  $|\delta\Omega_{12}|/M$  monotonically increases due to decay. This corresponds to moving the straight lines in Fig. 2 up (for  $\delta\Omega_{12} < 0$ ) or down (for  $\delta\Omega_{12} > 0$ ). Therefore decay invariably leads to the saddle-node bifurcation. This shows that the sharp drop of the scaled amplitude of mode 1 I is a generic effect, provided the system is initially close to the center that disappears at the bifurcation.

In Fig. 3(a) and (b) we show the time evolution of the scaled squared amplitudes of modes 1 and 2, I and M-I, for the same parameter values as in Fig. 4 of the main text, but for the initial point close to the separatrix. The behavior of I and M-I in this case is similar to that in Fig. 4 (a) and (c) of the main text, respectively, except that the jump in I that occurs near the saddle-node bifurcation is less pronounced. For the initial phase value  $\phi(0) = \pi/2$ 

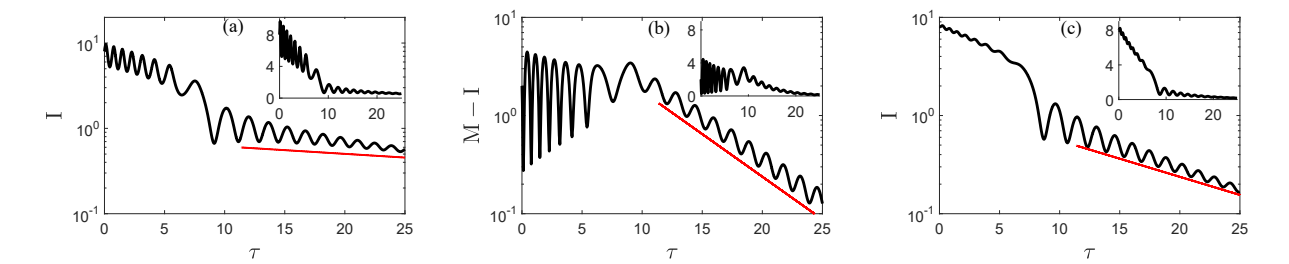


Figure 3. Time evolution of the amplitudes of the modes for small decay rates. The scaled squared amplitudes  $I=\omega_1A_1^2/3$  [panels (a) and (c)] and  $M-I=\omega_2A_2^2$  [panel (b)] of modes 1 and 2, respectively, are shown as functions of the scaled time  $\tau=3\gamma_{\rm res}t/4\omega_1^2$ . The main figure are on the logarithmic scale, the red lines show the exponential decay of I and M-I in the small-amplitude limit. The insets show the time evolution on the linear scale. The parameters are  $\delta\Omega_{12}=-5$ ,  $\mu_1=1$ , and M(0)=10, which corresponds to the parameter values in Fig. 3(a) of the main text. The initial values of the phase are  $\phi(0)=\pi/4$  in panels (a) and (b), and  $\phi(0)=0$  in panel (c); I(0)=8. The value  $\phi(0)=\pi/4$  corresponds to a trajectory that starts near the separatrix in Fig. 3(a) of the main text. The decay rates are  $4\omega_1^2\Gamma_1/3\gamma_{\rm res}=0.02$ ,  $\Gamma_2/\Gamma_1=5$  in panels (a) and (b); in panel (c)  $4\omega_1^2\Gamma_1/3\gamma_{\rm res}=0.05$  and  $\Gamma_2/\Gamma_1=1$ .

the behavior becomes similar to that in panel (b) of Fig. 4 of the main text. Figure 3(c) shows that the jump persists if we choose the decay rates to be equal.

### Mapping the decay-free dynamics on that of a particle in a potential well.

Time evolution of the scaled squared amplitude I of mode 1 in the absence of decay can be mapped onto the evolution of the coordinate of a particle with a unit mass, which oscillates in a potential well. These oscillations are described by equation

$$\frac{d^2I}{d\tau^2} = -\frac{\partial U_{\text{eff}}}{\partial I}, \qquad U_{\text{eff}}(I) = -\frac{1}{2}I^3(M-I) + \frac{1}{2}\left[h - \delta\Omega_{12}I - \frac{1}{2}\mu_1I^2 - \frac{1}{2}\mu_2(M-I)^2\right]^2, \tag{4}$$

where h is the value of the Hamiltonian (1). Equation (4) is derived from Eq. (1) and the Hamiltonian equations of motion for I and  $\phi$ , Eq. (5) of the main text.

The potential  $U_{\rm eff}$  is a quartic polynomial in I. It can have one well or two wells separated by a local maximum. The centers and the saddle point on the phase portraits in Fig. 3 of the main text correspond to  $\partial U_{\rm eff}/\partial I=0$ ; note, however, that these points on the phase portrait have different values of h, whereas  $U_{\rm eff}(I)$  depends on h as a parameter. It is important that the oscillations of  $I(\tau)$  in the potential  $U_{\rm eff}(I)$  occur with zero effective total energy,  $\frac{1}{2}(dI/d\tau)^2 + U_{\rm eff}(I) = 0$ , as again can be seen from Eq. (5) of the main text. Therefore Eq. (4) can be reduced to equation

$$\frac{dI}{d\tau} = \pm [-2U_{\text{eff}}(I)]^{1/2}.$$
 (5)

The sign  $\pm$  reflect the change of the sign of  $dI/d\tau$  at the turning points.

An immediate consequence of Eqs. (4) and (5) is that the time evolution of the scaled squared amplitude  $I(\tau)$  is described by Jacobi elliptic functions<sup>1</sup>. This shows, in particular, that in the case of a double-well potential the frequencies of vibrations in the both wells are equal. One of these vibrations corresponds to motion along a trajectory that circles around a center in Fig. 3(a) and (b) of the main text, whereas the other corresponds to motion along an open trajectory beneath the separatrix loop; both trajectories have the same value of h. The explicit expressions for  $I(\tau)$  simplify the calculation of its the period-averaged value away from the separatrix.

## References

1. Abramowitz, M. & Stegun, I. A. *Handbook of Mathematical Functions with Formulas, Graphs, and Mathematical Table* (Dover Publications, Inc., 1972).